Moroccan Journal of Chemistry
ISSN : 2351-812X

Mor. J. Chem., 2023, Volume 11, Issue 01, Page 144-154
https://revues.imist.ma/index.php/morjchem

The Synthesis, Characterisation, and Adsorption Study of Novel 4-Ethyl-3-Thisemicarbazone Microcrystalline Cellulose

Sahani N. I.[2], Mohamed A. H.[2], Ahmad N. M.[2], Sheikh Mohd Ghazali S. A. I.[1,2], Sharif I.[3], Dzulkifli N. N.[1,2*]

[1]*Material, Inorganic, and Oleochemistry (MaterInOleo) Research Group, School of Chemistry and Environment, Faculty of Applied Sciences, Universiti Teknologi MARA Cawangan Negeri Sembilan, Kampus Kuala Pilah, Pekan Parit Tinggi, 72000 Kuala Pilah, Negeri Sembilan, Malaysia*

[2]*School of Chemistry and Environment, Faculty of Applied Sciences, Universiti Teknologi MARA Cawangan Negeri Sembilan, Kampus Kuala Pilah, Pekan Parit Tinggi, 72000 Kuala Pilah, Negeri Sembilan, Malaysia*

[3]*Electron Microscopy Unit, Faculty of Science and Technology, Universiti Kebangsaan Malaysia, 43600 Bangi, Selangor, Malaysia*

**Corresponding author, Email address:* nurnadia@uitm.edu.my

Received *30 Oct 2022,*
Revised *28 Dec 2021,*
Accepted *05 Jan 2023*

Citation*: Sahani N. I., Mohamed A. H., Ahmad N. M., Sheikh Mohd Ghazali S.A.I., Sharif I., Dzulkifli, N. N. (2023) The synthesis, characterisation, and adsorption study of novel 4-ethyl-3-thisemicarbazone microcrystalline cellulose, Mor. J. Chem., 14(1), 144-154. Doi: 10.48317/IMIST.PRSM/morjchem-v11i1.32551*

Abstract: Cellulose is a linear glucose polymer manufacturable from various sources via different methods. Under the right conditions, small amounts of cellulose are transformed into derivatives that could be utilised to produce numerous commercial products. The selective cleavage of the C2-C3 bonds in anhydroglucose units in cellulose chains with a strong oxidant, namely sodium periodate ($NaIO_4$), produces dialdehyde cellulose (DAC). In the present study, DAC was reacted with 4-ethyl-3-thiosemicarbazide to produce 4-ethyl-3-thiosemicarbazone microcrystalline cellulose (TSCMCC). The structures of microcrystalline cellulose (MCC), DAC, and TSCMCC were characterised through FTIR, FESEM-EDX, XRD, and TGA. The υ(C=O) stretching band observed at 1728 cm^{-1} proved that DAC was successfully formed, while the bands at 1632 and 1225 cm^{-1} were correlated to υ(C=N) and υ(C=S) in TSCMCC. The FESEM revealed that the MCC were in bundles arrangement, the DAC was rod-shaped, and TSCMCC was needle-like. The EDX analysis showed sulphur (S) and nitrogen (N) atoms were present only in the TSCMCC. TSCMCC recorded the largest crystallite compared to MCC and DAC. Moreover, the TGA results exhibited that TSCMCC had lower thermal stability than MCC but higher than DAC. The zinc(II) ion adsorption capabilities of TSCMCC were assessed with ultraviolet-visible (UV-Vis) fitted with Langmuir and Freundlich isotherms.

Keywords: Cellulose; Dialdehyde cellulose; Thiosemicarbazone; Microcrystalline cellulose

1. Introduction

Cellulose is the fibrous carbohydrate found in plants. The compound is the most important natural polymer, recording 50 billion tonnes of biomass production annually (Thang *et al.*, 2017). Cellulose is a recyclable, biodegradable, and affordable basic material with appealing biomaterial properties (Ummartyotin and Manuspiya 2015). Each anhydroglucose unit (AGU) comprises 1,4-glucan cellulose hydroxyl groups at the C2, C3, and C6 of the cellulose. The CH_2OH group is situated at the C4 and C5 bonds and exhibited shear relativity with the O5 and C5 bonds (Liu *et al.*, 2021). Currently, heavy metal contamination has harmed the long-term development of aquatic flora and

fauna in polluted areas (Errich *et al*., 2021). Consequently, cellulose is a natural adsorber of various chemicals, including organic molecules, metal ions, and dyes. Nevertheless, the natural efficiency of cellulose adsorption is low, which could be improved with chemical modifications (Amini Horri *et al*., 2016). The most proficient technique for generating new materials with novel structures and properties is chemically modifying polysaccharides (Saygili and Guzel, 2017). Oxidation of cellulose is among the most frequently employed methods of converting cellulose into a value-added product (Coseri, 2017). In the technique, periodate is commonly utilised to disrupt the C2-C3 bond by selectively oxidising vicinal hydroxyl groups and yield two aldehyde groups. The aldehyde groups would then operate as cellulose modifying anchoring groups (Mendoza *et al.*, 2019).

Schiff base compounds are chemicals containing an imine group (-RC=N-) as the functional group, in which the nitrogen (N) atom is attached to an aryl or alkyl group (R) instead of hydrogen (Omidi and Kakanejadifard, 2020). Thiosemicarbazones are Schiff base derivatives that could attach to numerous transition metal ions via sulphur (S) and hydrazine N atoms, acting as versatile multi-dentate chelating ligands (Noruzi *et al.*, 2020). Furthermore, due to the numerous donor sets of S and N, thiosemicarbazones are employed as chelating ligands to form metal complexes (Prajapati and Patel, 2019). Consequently, thiosemicarbazone has the potential to be utilised to modify cellulose. Thiosemicarbazone-modified cellulose demonstrated an improved number of active sites, mechanical strength, and thermal stability (Vu *et al.*, 2020). Additionally, modified cellulose demonstrated higher adsorption efficiency than activated carbons and zeolites in removing heavy metal ions (Nguyen *et al.*, 2020, Fan *et al.*, 2002). In the current study, dialdehyde microcrystalline cellulose (DAC) was prepared through oxidation and reacted with 4-ethyl-3-thiosemicarbazide to modify the cellulose to acquire a novel 4-ethyl-3-thiosemicarbazone microcrystalline cellulose (TSCMCC). The TSCMCC was then evaluated as an adsorbent for the removal of zinc(II) [Zn(II)] ions.

2. Materials and Method

In the current study, the chemical reagents employed to prepare DAC and TSCMCC were microcrystalline cellulose (MCC), sodium periodate ($NaIO_4$), ethylene glycol, 4-ethyl-3-thiosemicarbazide, and zinc nitrate ($ZnNO_3$) was utilised in the adsorption study. Fourier transform infrared radiation (FTIR), field emission scanning electron microscopy (FESEM) with energy dispersive X-ray (EDX), X-ray diffraction (XRD), thermal gravimetric analysis (TGA), and ultraviolet-visible (UV-Vis) were also employed in the present study.

2.1 Ultrasonication of MCC

In a 250 mL conical flask, 10 g of MCC was dissolved in 200 mL of deionised water. The solution was subsequently treated with an ultrasound generator at 23–25 kHz, 500 W, and 35ºC for 45 minutes.

2.2 Oxidation of MCC

The $NaIO_4$ and pre-treated cellulose mixture was shaken gently for two hours at 40ºC in dark conditions to initiate the oxidation reaction. The oxidation was terminated by incorporating the mixture into 10 mL of 10% aqueous ethylene glycol solution and agitating it for 30 minutes. After the solution was left for 48 hours, the oxidised cellulose was filtrated, washed with deionised water, and oven-dried at 50ºC for 24 hours.

2.3 Synthesising TSCMCC

The thiourea group was grafted onto the cellulose by mixing the oxidised cellulose with 0.2 g of 4-ethyl-3-thiosemicarbazide at 65ºC for 30 minutes. The mixture was then refluxed at 60ºC for five hours

to acquire TSCMCC. Finally, the product was filtrated and washed with deionised water before being oven-dried.

2.4 Adsorption of heavy metal

Varying concentrations (1, 2, 3, 4, and 5 ppm) of $ZnNO_3$ solution were prepared. Subsequently, 0.01 g of TSCMCC was added to 10 mL of 1 ppm $ZnNO_3$, mixed, and subjected to a water bath shake at 50–60ºC and 115 rpm for two hours. After that, the resultant mixture was subjected to centrifugation for 10 minutes before being filtered. The procedure was repeated for the remaining concentrations of $ZnNO_3$.

3. Results and Discussion

3.1 The FTIR analysis

The FTIR analysis provided information on the main functional groups present in the MCC, DAC, and TSCMCC. Figures 1 and 2 display the FTIR spectra of MCC, DAC, and TSCMCC. The υ(OH) stretching band was visible at the 3340 and 3341cm^{-1} of the MCC and DAC spectra, respectively (Dzulkifli *et al.*, 2020). Nonetheless, the OH group in DAC did not oxidise completely as only the C2-C3 bonds of the AGU were selectively broken during oxidation with $NaIO_4$, producing two aldehyde groups at the designated positions through a cyclic iodate diester. Consequently, the two secondary hydroxyl groups were selected rather than the primary hydroxyl groups in the cellulose (Keshk *et al.*, 2019).

A stretching band corresponding to the aldehyde group, υ(C=O), was observed at 1728 cm^{-1}, demonstrating that the DAC was synthesised effectively (Madivoli *et al.*, 2019). The DAC was reacted with 4-ethyl-3-thiosemicarbazide to generate a new TSCMCC derivative. The TSCMCC spectrum exhibited a new stretching band at 1632 cm^{-1}, which contributed to υ(C=N) of the thiosemicarbazone moiety (Ezzat *et al.*, 2022). Additionally, a stretching band around 1232 cm^{-1} linked to the (C=S) bond was observed (Jawaria *et al.*, 2022). The reactions did not affect the cellulose backbone characteristics as all MCC stretching bands were still present on the DAC and TSCMCC spectra. The schematic reaction of 4-ethyl-3-thiosemicarbazone microcrystalline cellulose (TSCMCC) as shown in Scheme 1.

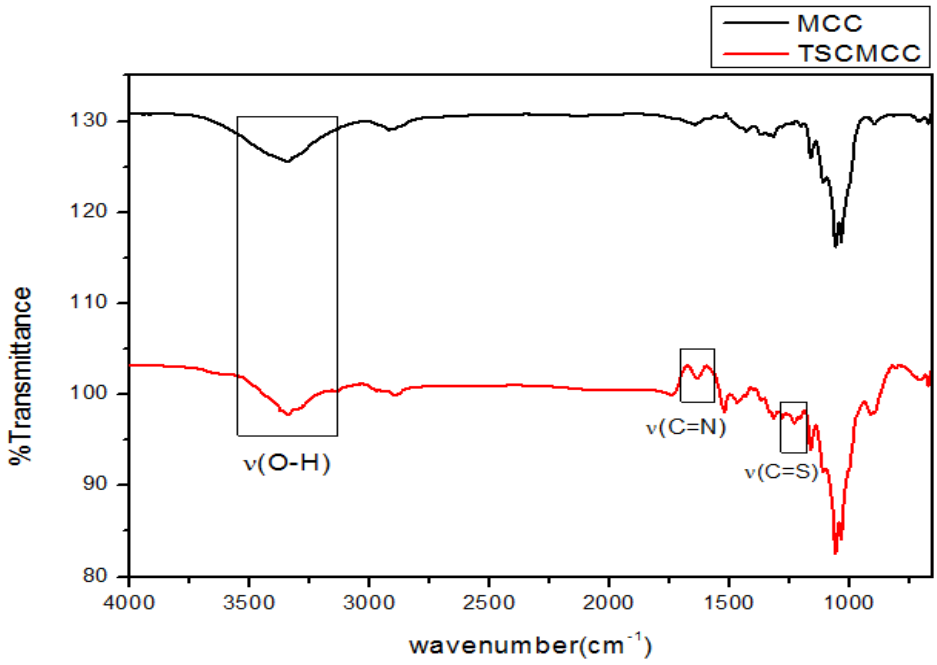

Figure 1. The FTIR spectra of the MCC and TSCMCC

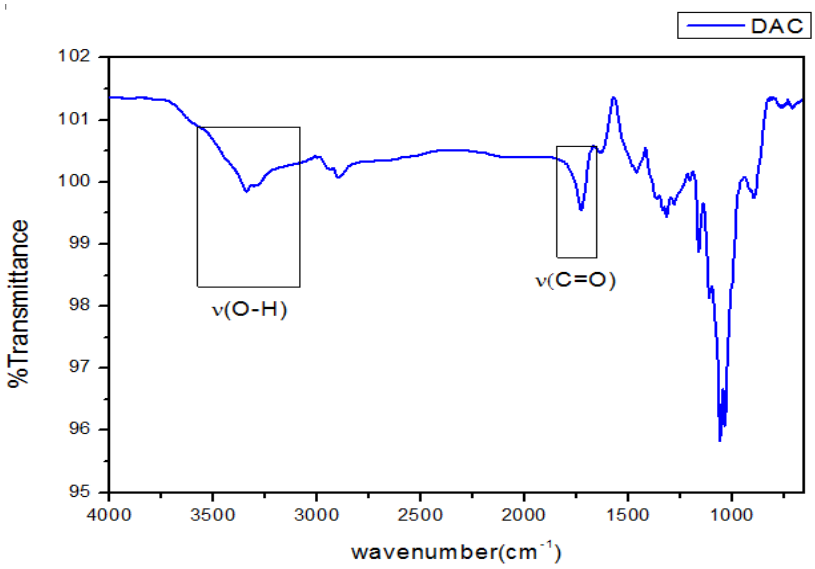

Figure 2. The FTIR spectrum of the DAC

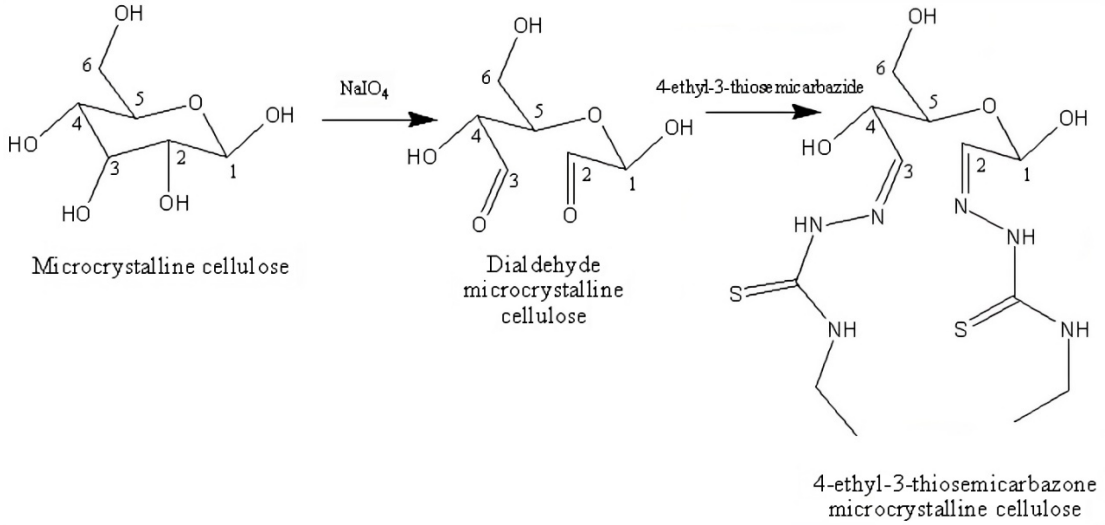

Scheme 1. The schematic formation of TSCMCC

3.2. The FESEM study

In the present study, FESEM was utilised to reveal the morphological features of the MCC, DAC, and TSCMCC. Generally, the surface of MCC was level and shiny. Non-cellulosic components that adhered to the surfaces of the fibres, such as lignin, hemicellulose, and silica, were successfully removed, hence resulting in a smooth surface (Galiwango *et al.*, 2019). The oxidation process with $NaIO_4$ generated morphological changes in MCC, resulting in a more compact cellulose texture. The DAC demonstrated visible kinks on the fibre (Adam *et al.*, 2019, Salleh *et al.*, 2017). Figure 3 displays the rod and rough form of the DAC. Conversely, TSCMCC exhibited needle-like morphological features upon the incorporation of 4-ethyl-3-thiosemicarbazide.

The elemental compositions of the selected region were assessed with energy dispersive X-ray (EDX) analysis coupled with FESEM. Figure 4 illustrates the chemical compositions of TSCMCC, which demonstrated 20.5 wt% S and 4.4 wt% N. The significant components observed in the cellulose were oxygen (17.3 wt%) and carbon (57.7 wt%). The S and N contents in the needle-shaped spots were high, most probably due to the 4-ethyl-3-thiosemicarbazone structure. The FTIR assessment exhibited stretching bands correlated to (C=N) and (C=S) bonds, thus indicating that TSCMCC was successfully synthesised.

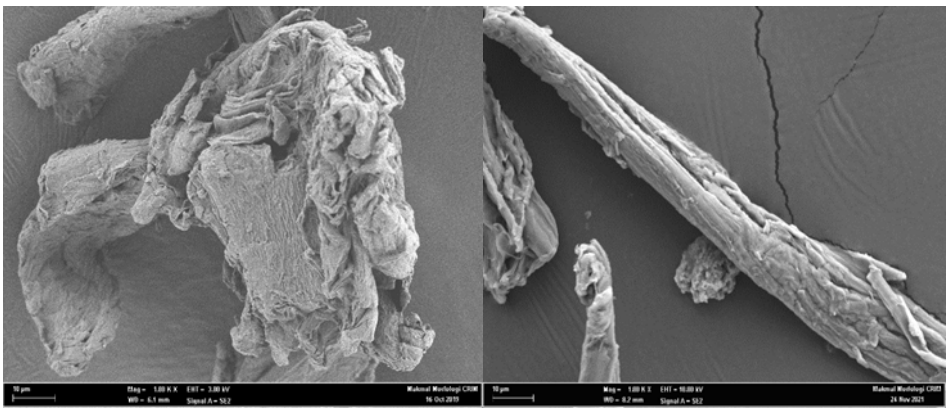

(a) (b)

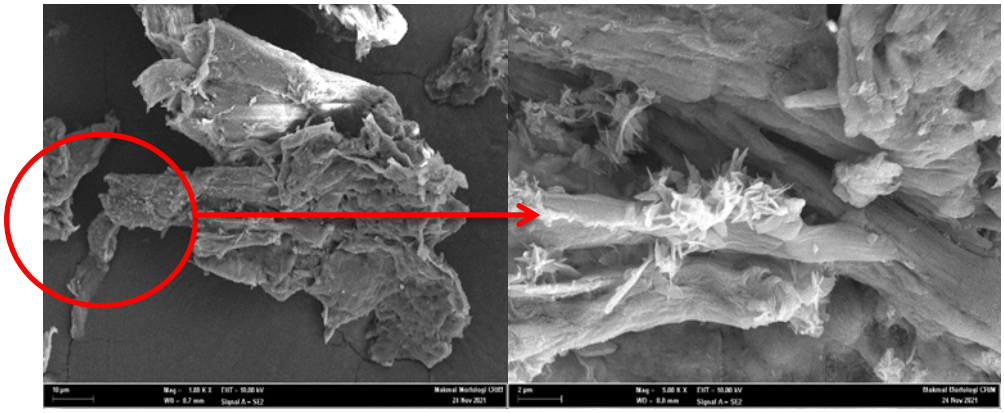

(c)

Figure 3. The FESEM micrographs of (a) MCC, (b) DAC, and (c) TSCMCC surfaces with 5000× magnification

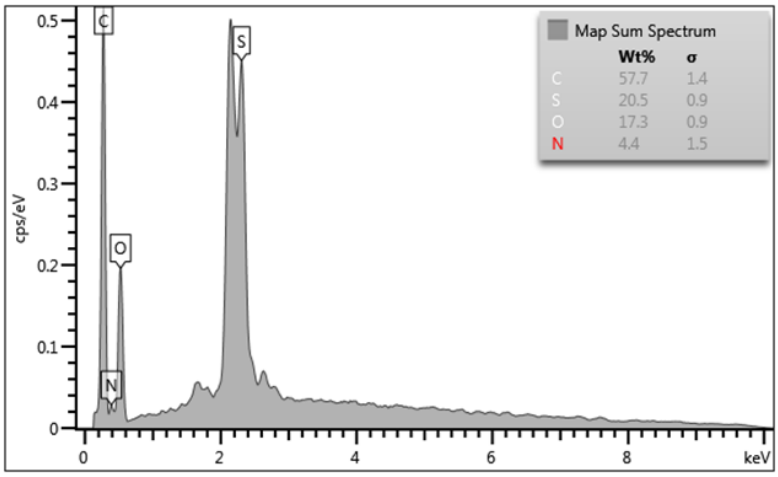

Figure 4. The EDX analysis of TSCMCC

3.3. The XRD analysis

The changes in the crystallinity of the MCC, DAC, and TSCMCC were evaluated with XRD as shown in Figure 5. The XRD data revealed that MCC, DAC, and TSCMCC recorded identical peaks within the 15–20º, 20–25º, and 30–35º ranges albeit with dissimilar 2Θ values. The intensities of the DAC peaks were lessened post oxidation of MCC with $NaIO_4$. Moreover, the cleavages at the C2-C3 bonds that produced dialdehyde groups reduced the crystallinity percentage of DAC. The TSCMCC

demonstrated the lowest crystallinity percentage compared to MCC and DAC. The observation was attributable to the new elements, S and N atoms of the thiosemicarbazone moiety, present in the TSCMCC structure. The crystallite size could also be obtained by substituting the full width at half maximum (FWHM) with the 2Θ value in the Scherer equation. Based on the equation, the crystallite sizes of MCC, DAC, and TSCMCC within the 20–25º range were 3.17, 3.10, and 3.66 nm, respectively. The 4-ethyl-3-thiosemicarbazone structure was substituted into the DAC, expanding the molecular size of TSCMCC and resulting in a more compact structure. Accordingly, the TSCMCC possessed the largest molecular size.

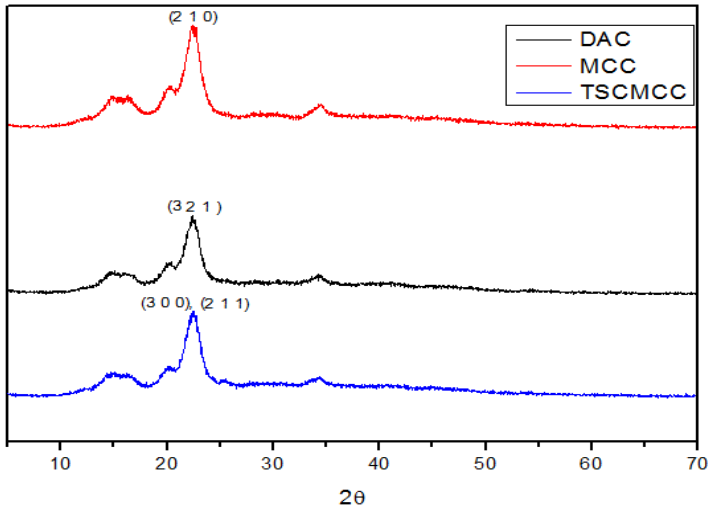

Figure 5. The XRD diffractograms of MCC, DAC, and TSCMCC

3.4. The TGA

Figure 6 illustrates the MCC, DAC, and TSCMCC TGA curves. The analysis was employed to assess the stability of the compounds at high temperatures. The MCC and DAC were fully degraded at 323.01°C and 316.89°C, respectively, with 86.9 and 70.5% weight losses. The end products of MCC and DAC were possibly charcoal powder, carbon dioxide (CO_2), and water (H_2O).

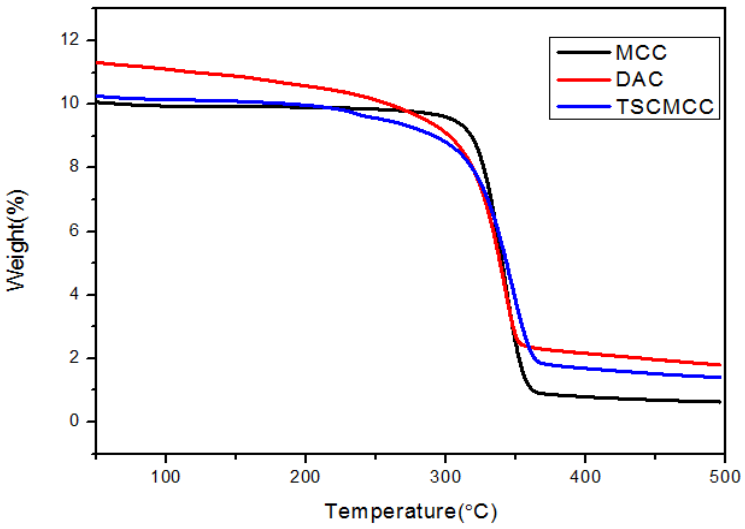

Figure 6. TGA thermograms of MCC, DAC, and TSCMCC

The dehydration indicated that the TSCMCC structure initially broke down at 213.41°C, while at 321.45°C, the compound was fully decomposed and lost 73.50% of its mass. The end products of TSCMCC were most likely charcoal powder, CO_2, sulphur dioxide (SO_2), nitrogen dioxide (NO_2),

and H_2O. The TSCMCC was more stable than MCC from adding 4-ethyl-3-thiosemicarbazone moiety into the cellulose structure. Meanwhile, the C2 and C3 bonds cleavages weakened the stability of DAC, which was less stable compared to MCC.

3.5. The Zn(II) ions adsorption study with UV-Vis

The UV-Vis spectroscopy was performed to examine the adsorption of Zn(II) ions with the compounds synthesised in the present study. The absorption spectrum of Zn(II) ion solution was measured within the wavelength region of 200–220 nm against a reagent blank. A linear graph of standard solution concentrations versus residual absorbance of Zn(II) ion after adding TSCMCC as an adsorbent is displayed in Figure 7. The linearity, R^2, of the graph was 0.9967, and the absorbance was directly proportional to the concentration. The adsorption capacity, q_e, and removal percentage were calculated according to Equations 1 and 2 (Abiaziem *et al.*, 2019, Costa *et al.*, 2015). Table 1 summarises the Zn(II) removal percentage. In the present study, the adsorption increased as the concentration was elevated. Consequently, TSCMCC exhibited the potential to be utilised as a new adsorbent for Zn(II) ion removal.

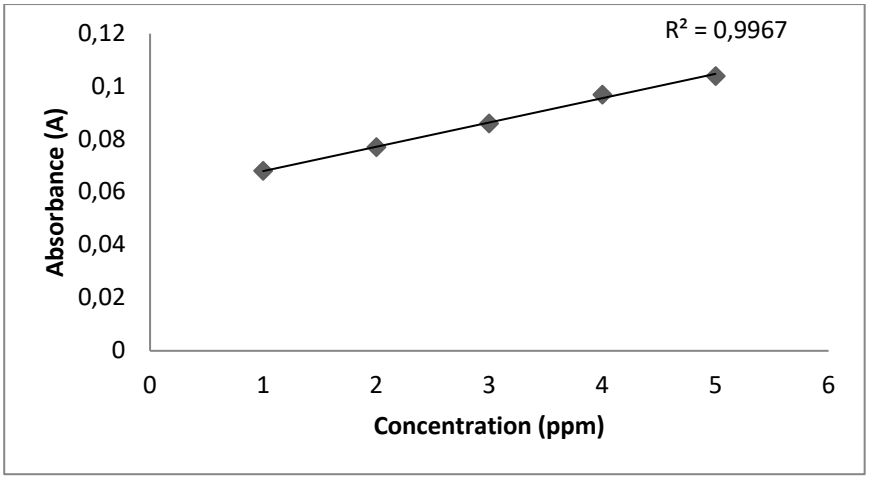

Figure 1. The graph of concentration $ZnNO_3$ versus absorbance upon adding TSCMCC

Table 1. The summary of percentage of Zn(II) ion removal

C_o (ppm)	C_e (ppm)	q_e	R%
1	0.10	0.09	90%
2	0.20	0.18	90%
3	0.30	0.27	90%
4	0.41	0.36	89%
5	0.50	0.45	90%

The ability was attributable to the variety of functional groups, including are azomethine (C=N) and thione (C=S), in the compound that could create covalent connections with the metal ions (O'Connell *et al.*, 2008):

$$q_e = \frac{(c_o - c_e)V}{w} \qquad \text{(Equation 1)}$$

$$R\% = \frac{c_o - c_e}{c_o} \times 100 \qquad \text{(Equation 2)}$$

Where q_e is the capacity of one gram of the adsorbent at equilibrium (mg/g) (Equation 1) (Tatsumi *et al.*, 2021), C_o denotes the starting concentration of the Zn(II) (mg/L), C_e is the concentration of Zn(II)

residue (mg/L), w represents the dry weight of the TSCMCC as adsorbent (g), V denotes the solution volume (L), R% is the removed or adsorbed heavy metal, and R% represents the percentage of Zn(II) eliminated. The adsorption isotherms were determined with Langmuir (see Equation 3) and Freundlich (Equation 5) (M'barek *et al.*, 2022, Gago *et al.*, 2020) models, while the Langmuir isotherm constant was calculated based on Equation 4. The Langmuir and Freundlich plots of TSCMCC Zn(II) ions adsorption are exhibited in Figures 8 and 9. The R^2 of the Langmuir isotherm was greater than the Freundlich isotherm, at 1 and 0.9997, respectively (Shafiq *et al.*, 2021, Zannagui *et al.*, 2020). Nonetheless, both plots were the ideal design for demonstrating Zn(II) ions adsorption by TSCMCC. In the Langmuir isotherm model, adsorption was assumed to have occurred on a homogenous surface with a finite number of energetically equivalent sites until a complete monolayer coverage was achieved (Lazzari *et al.*, 2021, Ayawei *et al.*, 2017, Muhammad and Abdurrahman, 2020).

$$\frac{1}{q_e} = \frac{1}{Q_m b c_e} v \qquad \text{(Equation 3)}$$

$$R_L = \frac{1}{1+(1+bc_o)} \qquad \text{(Equation 4)}$$

$$\ln q_e = \ln k_f + \frac{1}{n} \ln c_e \qquad \text{(Equation 5)}$$

Where q_e is the quantity of Zn(II) adsorbed per gram of the adsorbent (mg/L) (Equation 3), Q_m represents the maximum cover volume of the adsorbent (mg/g), b denotes Langmuir isotherm constant (L/mg), C_e is the concentration of the metal ion at equilibrium (mg/L), q_e represents the amount of metal adsorbed of the adsorbent at equilibrium (mg/g) (Equation 5), n denotes the adsorption intensity, and k_f is the Freundlich isotherm constant. According to the Langmuir isotherm, adsorption occurs when Zn(II) ions come into contact with the surface of TSCMCC. The values of R_L in TSCMCC adsorption of Zn(II) ions ranged from 0.4704 to 0.4938. Values of less than 1 indicate an excellent adsorption process and that the adsorbent possessed a good affinity for the uptake of Zn(II) ions. Similarly, the Freundlich isotherm expresses good adsorption characteristics on heterogeneous surfaces (Kali *et al.*, 2022). In the current study, the adsorption intensity, n, obtained from the Freundlich isotherm graph was 0.9997, denoting the adsorption process and the affinity of the adsorbent for Zn(II) ions were excellent.

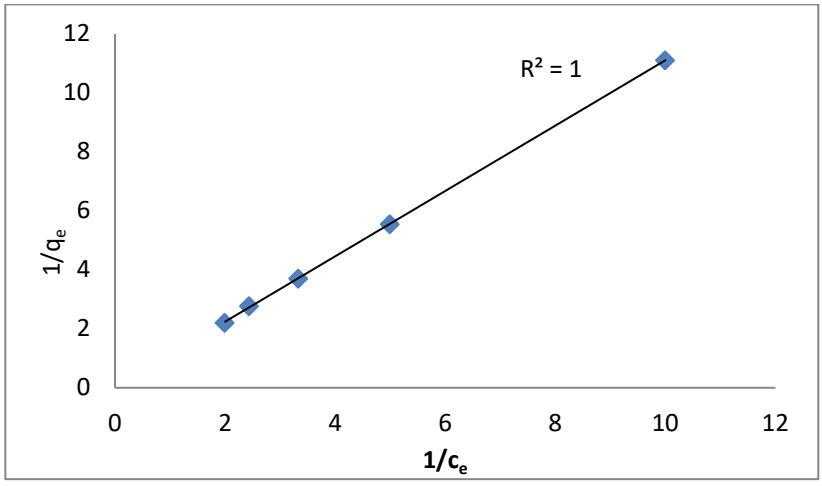

Figure 8. The Langmuir isotherm graph

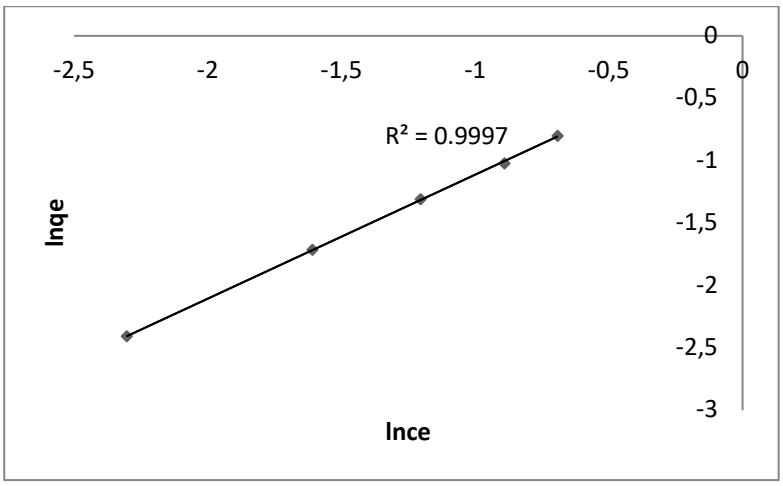

Figure 2. The Freundlich isotherm graph

Conclusion

In the present study, TSCMCC was successfully synthesised at 60ºC via reflux. The dialdehyde group in DAC was successfully removed and the formation of TSCMCC was proved by the presence of new stretching bands, υ(C=N) and υ(C=S), recorded in the FTIR spectra. Additionally, EDX confirmed the presence of thiosemicarbazone moiety in the microcrystalline cellulose, the needle-shaped structures recorded in FESEM. The XRD results demonstrated that the crystallinity of MCC was the highest, followed by DAC and TSCMCC. Additionally, the TSCMCC crystallites were the biggest compared to MCC and DAC. From the TGA assessment, TSCMCC has better stability than MCC. Meanwhile, the stability of DAC was lower than MCC due to cleavage at the C2 and C3 bonds, which reduces DAC's stability. Lastly, for the adsorption study, the adsorption of TSCMCC is suited to Langmuir and Freundlich isotherms. The results showed that TSCMCC is a promising adsorbent since the separation factor, $R_{L,}$ was less than 1, while n was 1. Both isotherms indicate achievable and efficient adsorption.

Acknowledgements

The authors would like to express their gratitude to the Faculty of Applied Sciences, Universiti Teknologi MARA, Negeri Sembilan Branch, Kuala Pilah Campus, Negeri Sembilan, Malaysia for providing the research facilities, and UTM for the computational facility.

Disclosure statement: *Conflict of Interest:* The authors declare that there are no conflicts of interest.
Compliance with Ethical Standards: This article does not contain any studies involving human or animal subjects.

References

Abiaziem C. V., Williams A. B., Inegbenebor A. I., Onwordi C. T., Ehi-Eromosele C. O., Petrik L. F., (2019) Adsorption of lead ion from aqueous solution unto cellulose nanocrystal from cassava peel, *J. Phys. Conf. Ser.,* 1299, 012122

Adam N. A., Sheikh Mohd Ghazali S. A. I., Dzulkifli N. N., Hak C. R. C., Sarijo S. H., (2019) Intercalations and Characterization of Zinc/Aluminium Layered Double Hydroxide-Cinnamic Acid, *Bull. Chem. React. Eng.*, 14(1), 165-172. doi: https://doi.org/10.9767/bcrec.14.1.3328.165-172

Amini Horri B., Tan K. B., Abdullah A. Z., Salamatinia B., (2016) Adsorption Mechanism of Microcrystalline Cellulose as Green Adsorbent for the Removal of Cationic Methylene Blue Dye, *J. Chem. Soc. Pak.,* 38(4), 651-664

Ayawei N., Ebelegi A. N., Wankasi D., (2017) Modelling and Interpretation of Adsorption Isotherms, *J. Chem.,* 2017, 1-11. doi: https://doi.org/10.1155/2017/3039817

Coseri S., (2017) Cellulose: To depolymerize… or not to?, *Biotechnol. Adv.,* 35(2), 251-266. doi: https://doi.org/10.1016/j.biotechadv.2017.01.002

Costa T. D. S., Rogez H., Pena R. D. S., (2015) Adsorption capacity of phenolic compounds onto cellulose and xylan, *Food Sci. Technol.,* 35(2), 314-320. doi: http://dx.doi.org/10.1590/1678-457X.6568

Dzulkifli N. N., Zaki N. W. M., Mohamed A. H., Ahmad N. M., Sheikh Mohd Ghazali S. A. I., (2020) Study on the oxidation and properties of dihydroxyl cellulose using different amounts of sodium periodate, *Malaysian J. Anal. Sci.,* 24(6), 830-837

Errich A., Azzaoui K., Mejdoubi E., Hammouti B., Abidi N., Akartasse N., Benidire L., EL Hajjaji S., Sabbahi R., Lamhamdi A., (2021). Toxic heavy metals removal using a hydroxyapatite and hydroxyethyl cellulose modified with a new Gum Arabic, *Indonesian Journal of Science & Technology* 6(1), 41-64

Ezzat A., Mohamed M. B. I., Mahmoud A. M., Farag R. S., El-Tabl A. S., Ragab A., (2022) Synthesis, spectral characterization, antimicrobial evaluation and molecular docking studies of new Cu(II), Zn(II) thiosemicarbazone based on sulfonyl isatin, *J. Mol. Struct.,* 1251, 132004. doi: https://doi.org/10.1016/j.molstruc.2021.132004

Fan J., Zhang S., Xu Y., Wei N., Wan B., Qian L., Liu Y., (2020) A polyethylenimine/salicylaldehyde modified cellulose Schiff base for selective and sensitive Fe^{3+} detection, *Carbohydr. Polym.,* 228, 115379-115386. doi: https://doi.org/10.1016/j.carbpol.2019.115379

Gago D., Chagas R., Ferreira L. M., Velizarov S., Coelhoso I., (2020) A novel cellulose-based polymer for efficient removal of methylene blue, *Membranes,* 10(1), 13-29. doi: https://doi.org/10.3390/membranes10010013

Galiwango E., Rahman N. S. A., Al-Marzouqi A. H., Abu-Omar M. M., Khaleel A. A., (2019) Isolation and characterization of cellulose and α-cellulose from date palm biomass waste, *Heliyon,* 5(12), E02937-E02944. doi: https://doi.org/10.1016/j.heliyon.2019.e02937

Jawaria R., Khan M. U., Hussain M., Muhammad S., Sagir M., Hussain A., Al-Sehemi A. G., (2022) Synthesis and characterization of ferrocene-based thiosemicarbazones along with their computational studies for potential as inhibitors for SARS-CoV-2, *J. Iran. Chem. Soc.,* 19(3), 839-846. doi: https://doi.org/10.1007/s13738-021-02346-1

Kali A., Dehmani Y., Loulidi L., Amar A., Jabri M., El-kord A., Boukhlifi F., (2022) Study of the adsorption properties of an almond shell in the elimination of methylene blue in an aquatic, *Mor. J. Chem.,* 10N°3, 509-522. doi: http://dx.doi.org/10.48317/IMIST.PRSM/morjchem-v10i3.33140

Keshk S. M. A. S., Bondock S., El-Zahhar A. A., Haija M. A., (2019) Synthesis and characterization of novel Schiff's bases derived from dialdehyde cellulose-6-phosphate, *Cellulose,* 26, 3703-3712. doi: https://doi.org/10.1007/s10570-019-02360-w

Lazzari L. K., Perondi D., Zattera A. J., Santana R. M. C., (2021) Cellulose/Biochar Cryogels: A Study of Adsorption Kinetics and Isotherms, *Langmuir,* 37(10), 3180-3188. doi: https://doi.org/10.1021/acs.langmuir.1c00123

Liu Y., Ahmed S., Sameen D. E., Wang Y., Lu R., Dai J., Li S., Qin W., (2021) A review of cellulose and its derivatives in biopolymerbased for food packaging application, *Trends Food Sci. Technol.,* 112, 532-546. doi: https://doi.org/10.1016/j.tifs.2021.04.016

Madivoli E. S., Kareru P. G., Gachanja A. N., Mugo S. M., Makhanu D. S., (2019) Synthesis and characterization of dialdehyde cellulose nanofibers from O. sativa husks, *SN Appl. Sci.,* 1(7), 1-7. doi: https://doi.org/10.1007/s42452-019-0769-9

M'barek I., Slimi H., Abdulmohsen K. D. A., Alimi F., Lajimi R. H., Mechi L., ben Salem R., Moussaoui Y., (2022) Cellulose from Tamarix aphylla's stem via acetocell for cadmium adsorption, *Arab. J. Chem.* 15, 103679-103689. doi: https://doi.org/10.1016/j.arabjc.2021.103679

Mendoza D. J., Browne C., Raghuwanshi V. S., Simon G. P., Garnier G., (2019) One-shot TEMPO-periodate oxidation of native cellulose, *Carbohydr. Polym.,* 226, 1-25. doi: https://doi.org/10.1016/j.carbpol.2019.115292

Muhammad A. S., Abdurrahman M. A., (2020) Adsorption of Methylene blue onto modified Agricultural waste, *Mor. J. Chem.,* 8N°2, 412-427. doi: https://doi.org/10.48317/IMIST.PRSM/morjchem-v8i2.16692

Nguyen T. A., Tran D. B., Le H. D. C., Nguyen Q. L., Pham V., (2020) Thiosemicarbazone-Modified Cellulose: Synthesis, Characterization, and Adsorption Studies on Cu(II) Removal, *ACS Omega,* 5(24), 14481-14493. doi: https://doi.org/10.1021/acsomega.0c01129

Noruzi E. B., Shaabani B., Geremia S., Hickey N., Nitti P., Kafi H. S., (2020) Synthesis, Crystal Structure, and Biological Activity of a Multidentate Calix[4]arene Ligand Doubly Functionalized by 2-Hydroxybenzeledene-Thiosemicarbazone, *Molecules,* 25(2), 370-388. doi: https://doi.org/10.3390/molecules25020370

O'Connell D. W., Birkinshaw C., O'Dwyer T. F., (2008) Heavy Metal Adsorbents Prepared from the Modification of Cellulose: A Review, *Bioresour. Technol.,* 99(15), 6709-6724. doi: https://doi.org/10.1016/j.biortech.2008.01.036

Omidi S., Kakanejadifard A., (2020) A review on biological activities of Schiff base, hydrazone, and oxime derivatives of curcumin, *RSC Adv.* 10, 30186-30202. doi: https://doi.org/10.1039/D0RA05720G

Prajapati N. P., Patel H. D., (2019) Novel thiosemicarbazone derivatives and their metal complexes: Recent development, Synth. Commun., 49(21), 2767-2804. doi: https://doi.org/10.1080/00397911.2019.1649432

Salleh N. M., Mohsin S. M. N., Sarijo S. H., Sheikh Mohd Ghazali S. A. I., (2017) Synthesis and physico-chemical properties of zinc layered hydroxide-4-chloro-2-methylphenoxy acetic acid (ZMCPA) nanocomposite, *IOP Conf. Ser. Mater. Sci. Eng.,* 204, 012012

Shafiq M., Alazba A. A., Amin M. T., (2021) Kinetic and Isotherm Studies of Ni^{2+} and Pb^{2+} Adsorption from Synthetic Wastewater Using *Eucalyptus camdulensis*—Derived Biochar*, Sustainability*, 13(7), 3785-3800. doi: https://doi.org/10.3390/su13073785

Saygili G. A., Guzel F., (2017) Chemical modification of a cellulose-based material to improve its adsorption capacity for anionic dyes, J. Dispers. Sci. Technol., 38(3), 381-392

Tang Z., Li W., Lin X., Xiao H., Miao Q., Huang L., Chen L., Wu H., (2017) TEMPO-Oxidized Cellulose with High Degree of Oxidation, *Polymers.,* 9(9), 421-430. doi: https://doi.org/10.3390/polym9090421

Tatsumi T., Tahara Y., Matsumoto M., (2021) Adsorption of Metallic Ions on Amidoxime-Chitosan/Cellulose Hydrogels, *Separations,* 8, 202-210. doi: https://doi.org/10.3390/separations8110202

Ummartyotin S., Manuspiya H., (2015) A critical review on cellulose: From fundamental to an approach on sensor technology, *Renew. Sust. Energ. Rev.,* 41(C), 402-412. doi: https://doi.org/10.1016/j.rser.2014.08.050

Vu H. T., Phan M. T. D., Trab U. T. T., Nguyen G. D., Duong V. B., Tran D. B., (2020) N(4)-Morpholinothiosemicarbazide-Modified Cellulose: Synthesis, Structure, Kinetics, Thermodynamics, and Ni(II) Removal Studies, *ACS Omega,* 5(25), 15229-15239. doi: https://doi.org/10.1021/acsomega.0c01234

Zannagui C., Amhamdi H., El Barkany S., Jilal I., Sundman O., Salhi A., Chaouf S., Abou-Salama M., El Idrissi A., Zaghrioui M., (2020) Design, Characterization and Investigation of Heavy Metal Ions Removal by New Cellulose-Ether Based adsorbent, *Mor. J. Chem.,* 8N°1, 332-346

(2023) ; https://revues.imist.ma/index.php/morjchem/index